Indolicidin Binding Induces Thinning of a Lipid Bilayer

Chris Neale,[†‡] Jenny C. Y. Hsu,[‡§] Christopher M. Yip,[‡§] and Régis Pomès[†‡*]
[†]Molecular Structure and Function, The Hospital for Sick Children, Toronto, Ontario, Canada; [‡]Department of Biochemistry and [§]Terrence Donnelly Centre for Cellular and Biomolecular Research, University of Toronto, Toronto, Ontario, Canada

ABSTRACT   We use all-atom molecular dynamics simulations on a massive scale to compute the standard binding free energy of the 13-residue antimicrobial peptide indolicidin to a lipid bilayer. The analysis of statistical convergence reveals systematic sampling errors that correlate with reorganization of the bilayer on the microsecond timescale and persist throughout a total of 1.4 ms of sampling. Consistent with experimental observations, indolicidin induces membrane thinning, although the simulations significantly overestimate the lipophilicity of the peptide.

Antimicrobial peptides are a component of the innate immune system of eukaryotes (1). As such, they must interact with pathogenic membranes, either during translocation or by disrupting their structural integrity (2). Here we examine the binding of the 13-residue cationic antimicrobial peptide indolicidin (3) (ILPWKWPWWPWRR-NH$_2$) to a lipid membrane as a first step towards elucidating its mechanism of action.

Molecular solutes interact with lipid membranes in many cellular processes (4). Computational approaches such as molecular dynamics simulations have been widely used to characterize these interactions (5). However, molecular dynamics simulations can require unfeasibly long times to reach equilibrium (6). Therefore, it is common to compute equilibrium properties of solute insertion into lipid bilayers using umbrella sampling (7) simulations in which the solute is restrained along the bilayer normal using harmonic restraining potentials, or umbrellas, centered at z_i^0 values distributed between bulk water and the bilayer center.

It is often assumed that equilibrium properties rapidly attain convergence in umbrella sampling simulations; accordingly, convergence measures are rarely published (8). However, we have recently shown that umbrella sampling simulations require up to 100 ns per umbrella (3 μs in total) to eliminate systematic sampling errors in the standard free energy of binding, $\Delta G_{\mathrm{bind}}^0$, of an arginine side-chain analog from bulk water to a lipid bilayer (8). The fact that umbrella sampling has been used to investigate the bilayer insertion of substantially larger solutes (9) motivates a systematic evaluation of statistical sampling convergence of $\Delta G_{\mathrm{bind}}^0$ for indolicidin in a lipid bilayer.

To estimate $\Delta G_{\mathrm{bind}}^0$ of indolicidin to a lipid bilayer, we conducted 60 sets of umbrella-sampling simulations while systematically varying the initial conformation. In each umbrella sampling simulation, each umbrella was simulated for 1.5 μs, yielding a total simulation time of 1.4 ms and 60 independent free energy or potential of mean force (PMF) profiles from bulk water to the center of a POPC (1-palmitoyl-2-oleoyl-*sn*-glycero-3-phosphatidylcholine) lipid bilayer.

The PMF profiles indicate that indolicidin strongly binds to the bilayer, partitioning inside the lipid headgroups (Fig. 1, *A* and *E*). Importantly, the mean estimate of $\Delta G_{\mathrm{bind}}^0$ decays exponentially with equilibration time t_{eq}, indicating that systematic sampling errors in individual simulations continued to decrease throughout the 1.5-μs interval as rare events led to more favorable states (Fig. 1 *B*). The low frequency of transitions to more favorable states exacerbates the requirement for massive sampling using multiple independent simulations.

Computational limitations precluded extending all 60 sets of umbrella-sampling simulations to even longer times. Instead, we identified the two simulations at each umbrella that appeared to be most representative of equilibrium and extended each to 10 μs per umbrella (see Methods in the Supporting Material). The resulting estimates of $\Delta G_{\mathrm{bind}}^0$ continued to decrease until $t_{\mathrm{eq}} = 4$ μs (68 μs in total), after which they stabilized at the asymptotic limit of the exponential fit of the shorter simulation data ($\Delta G_{\mathrm{bind}}^0 = -26 \pm 5$ kcal/mol; Fig. 1 *C*).

As indolicidin approaches the bilayer, it is drawn closer (Fig. 2 *A*) as salt bridges form between the peptide and the phospholipid headgroups (Fig. 2 *B*), inducing their protrusion (Figs. 1 *D* and 2 *C*). At large separation distances, this state is attained only when the peptide becomes highly extended (Fig. 2, *D* and *E*). As indolicidin is inserted more deeply, the surface of the lipid bilayer invaginates (Figs. 1 *E* and 2 *C*), maintaining peptide-lipid salt bridges (Fig. 2 *B*) and leading to the formation of a pore when the solute is near the bilayer center (Figs. 1 *F* and 2 *C*, and see Fig. S2, Fig. S3, Fig. S4, and Fig. S5 in the Supporting
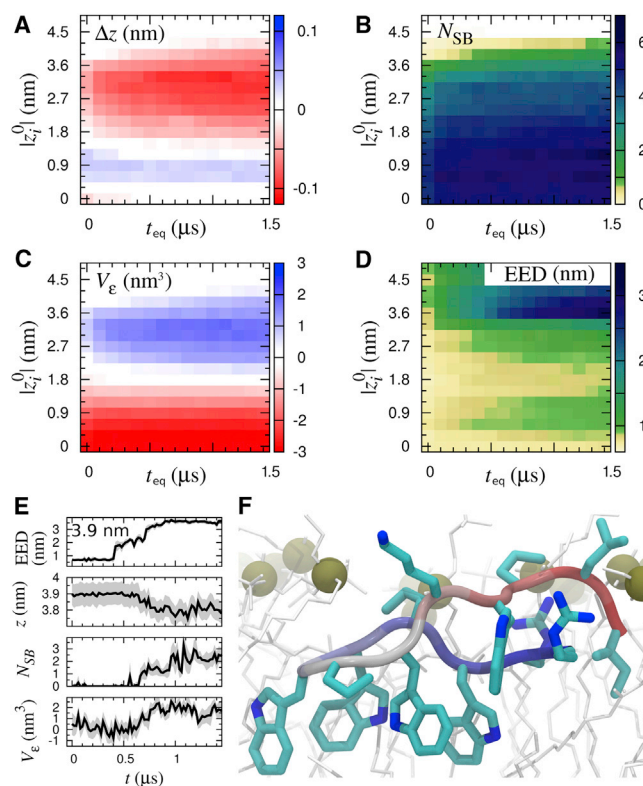

CrossMark
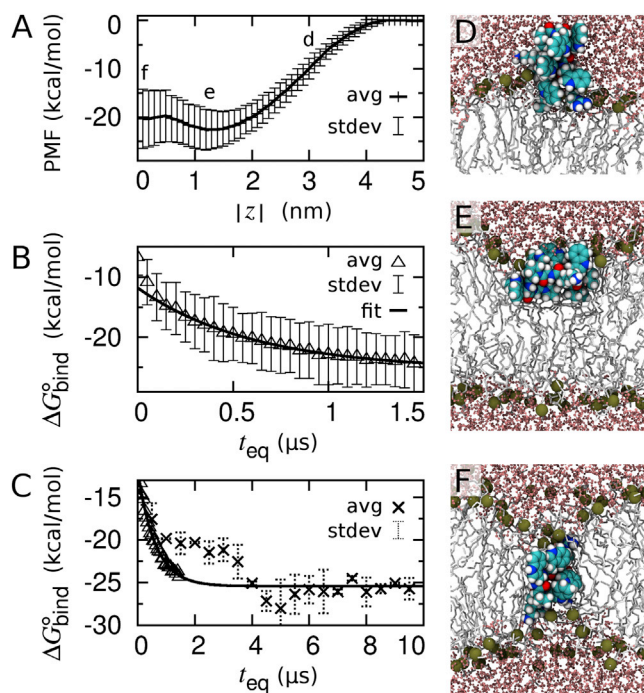
FIGURE 1 PMF for indolicidin partitioning into a POPC bilayer. (*A*) Average PMF from 60 independent umbrella-sampling simulations based on $1 < t \leq 1.5$ μs/umbrella. (*B*) Average ΔG^0_{bind} from 50-ns time intervals per umbrella ($t_{eq} < t \leq t_{eq}+50$ ns) as a function of equilibration time, t_{eq}. (*Solid line*) Single exponential fit to the mean over $0.5 < t_{eq} \leq 1.5$ μs. (*C*) Mean values of ΔG^0_{bind} from the 10-μs/umbrella simulations (*crosses*) together with the mean values of ΔG^0_{bind} (*triangles*) and exponential fit from panel *B*. PMF and ΔG^0_{bind} profiles obtained from each of the 60 independent simulations are shown in Fig. S1 in the Supporting Material. (*D–F*) Representative conformations after 1.5 μs of simulation at $z^0_i = $ (*D*) 3 nm, (*E*) 1.2 nm, and (*F*) 0.0 nm. To see this figure in color, go online.

FIGURE 2 Slow equilibration of bilayer and peptide. (*A–D*) Color quantifies conformational reorganization for $t_{eq} < t \leq t_{eq} + 100$ ns as a function of t_{eq} and $|z^0_i|$. (*A*) Deviation of insertion depth, z, from z^0_i, $\Delta z \equiv z - z^0_i$; (*B*) number of peptide-lipid salt bridges, N_{SB}; (*C*) volume change of the bilayer's proximal leaflet in the radial vicinity of the solute, V_ε; and (*D*) peptide end-to-end distance (EED). There is no sampling for $t > 0.5$ μs at $|z^0_i| \geq 4.5$ nm. (*E*) Representative time-series of a trajectory at $z^0_i = 3.9$ nm. (*F*) Representative conformation at 10 μs for $|z^0_i| = 1.2$ nm. To see this figure in color, go online.

Material). These Boltzmann-weighted ensemble averages may not be mechanistically representative of nonequilibrium binding events (8,10).

The reorganization of the peptide, the bilayer, and the ionic interactions between them became more pronounced with increasing simulation time at peptide insertion depths shallower than the global free energy minimum ($|z^0_i| > 1.4$ nm; Fig. 1 *A* and Fig. 2, *B–D*). These conformational transitions are likely the source of the systematic drift of ΔG^0_{bind}. Reorganization of the bilayer also controls the rate of equilibration during membrane insertion of an arginine side chain (8,9) and a cyclic arginine nonamer (11), suggesting that slow reorganization of lipids around cationic solutes presents a general impediment to simulation convergence.

Consistent with the perturbation of membrane thickness observed by in situ atomic force microscopy (12), our results suggest that indolicidin insertion induces local thinning of the bilayer (Fig. 1, *E* and *F*, and Fig. 2, *C* and *F*). The different conformational ensembles sampled by the

peptide in water and in the lipid bilayer (Fig. 2 *D*) are consistent with the observations that indolicidin is disordered in solution (13) and adopts stable conformations in the presence of detergent (14). Although the peptide's conformation continued to change when it was deeply inserted (Fig. 2 *D*), the amount of water in the bilayer's hydrophobic core converged relatively rapidly (see Fig. S2). Indolicidin can induce the formation of hydrated, porelike defects (see Fig. S2, Fig. S3, Fig. S4, and Fig. S5) but does not act as a chloride carrier (see Fig. S6 and Fig. S7). Future studies of the mechanism of indolicidin action will examine the effect of multiple peptide binding.

The PMF profile presented in this Letter is strikingly different from that computed by Yeh et al. (15) using different force field parameters for indolicidin partitioning into a DMPC (1,2-dimyristoyl-*sn*-glycero-3-phosphatidylcholine) bilayer, from which the binding free energy was estimated to be 0 kcal/mol (15). However, that study comprised only 25 ns per umbrella and likely suffers from systematic sampling errors induced by initial conditions (see Fig. S8).

Our estimate of the binding affinity is much larger than the values obtained for indolicidin and large unilamellar POPC vesicles using isothermal titration calorimetry, −7.4 kcal/mol (16), and equilibrium dialysis, −8.8 kcal/mol (13). Such a discrepancy suggests that the relative accuracy of binding free energies for amino-acid side-chain analogs (8,9,17) does not necessarily extend to polypeptides. Although more work is needed to elucidate the source of this discrepancy, this study underlines the importance of attaining convergence before evaluating force-field accuracy.

Importantly, this work also highlights the extensive sampling required to remove systematic errors induced by initial conditions in atomistic simulations of peptides in membranes. Slow equilibration of the system is due to rare transitions across hidden free energy barriers involving reorganization of the membrane. Two simple recommendations are 1), evaluating the time-dependence of ensemble averages, and 2), conducting multiple simulations with different initial conditions. We have recently shown that by using enhanced sampling techniques it is possible to identify the locations of hidden free energy barriers without a priori knowledge (9). Future research will examine strategies for speeding up the crossing of these barriers, such as optimized order parameters including bilayer reorganization and enhanced sampling techniques including a random walk along the order parameter (9).

SUPPORTING MATERIAL

Supplemental Methods and Results, two tables, eight figures, three equations and references (18–24) are available at http://www.biophysj.org/biophysj/supplemental/S0006-3495(14)00275-6.

ACKNOWLEDGMENTS

REFERENCES and FOOTNOTES

1. Hancock, R. E. W. 2001. Cationic peptides: effectors in innate immunity and novel antimicrobials. *Lancet Infect. Dis.* 1:156–164.

2. Epand, R. M., and H. J. Vogel. 1999. Diversity of antimicrobial peptides and their mechanisms of action. *Biophys. Biochim. Acta.* 1462: 11–28.

3. Selsted, M. E., M. J. Novotny, …, J. S. Cullor. 1992. Indolicidin, a novel bactericidal tridecapeptide amide from neutrophils. *J. Biol. Chem.* 267:4292–4295.

4. Stein, W. 1986. Transport and Diffusion across Cell Membranes. Academic Press, Orlando, FL.

5. Saiz, L., and M. L. Klein. 2002. Computer simulation studies of model biological membranes. *Acc. Chem. Res.* 35:482–489.

6. Grossfield, A., S. E. Feller, and M. C. Pitman. 2007. Convergence of molecular dynamics simulations of membrane proteins. *Proteins.* 67:31–40.

7. Torrie, G. M., and J. P. Valleau. 1977. Nonphysical sampling distributions in Monte Carlo free-energy estimation: umbrella sampling. *J. Comput. Phys.* 23:187–199.

8. Neale, C., W. F. D. Bennett, …, R. Pomès. 2011. Statistical convergence of equilibrium properties in simulations of molecular solutes embedded in lipid bilayers. *J. Chem. Theory Comput.* 7:4175–4188.

9. Neale, C., C. Madill, …, R. Pomès. 2013. Accelerating convergence in molecular dynamics simulations of solutes in lipid membranes by conducting a random walk along the bilayer normal. *J. Chem. Theory Comput.* 9:3686–3703.

10. Kopelevich, D. I. 2013. One-dimensional potential of mean force underestimates activation barrier for transport across flexible lipid membranes. *J. Chem. Phys.* 139:134906.

11. Huang, K., and A. E. García. 2013. Free energy of translocating an arginine-rich cell-penetrating peptide across a lipid bilayer suggests pore formation. *Biophys. J.* 104:412–420.

12. Shaw, J. E., J.-R. Alattia, …, C. M. Yip. 2006. Mechanisms of antimicrobial peptide action: studies of indolicidin assembly at model membrane interfaces by in situ atomic force microscopy. *J. Struct. Biol.* 154:42–58.

13. Ladokhin, A. S., M. E. Selsted, and S. H. White. 1997. Bilayer interactions of indolicidin, a small antimicrobial peptide rich in tryptophan, proline, and basic amino acids. *Biophys. J.* 72:794–805.

14. Rozek, A., C. L. Friedrich, and R. E. W. Hancock. 2000. Structure of the bovine antimicrobial peptide indolicidin bound to dodecylphosphocholine and sodium dodecyl sulfate micelles. *Biochemistry.* 39:15765–15774.

15. Yeh, I.-C., D. R. Ripoll, and A. Wallqvist. 2012. Free energy difference in indolicidin attraction to eukaryotic and prokaryotic model cell membranes. *J. Phys. Chem. B.* 116:3387–3396.

16. Andrushchenko, V. V., M. H. Aarabi, …, H. J. Vogel. 2008. Thermodynamics of the interactions of tryptophan-rich cathelicidin antimicrobial peptides with model and natural membranes. *Biochim. Biophys. Acta.* 1778:1004–1014.

17. MacCallum, J. L., W. F. D. Bennett, and D. P. Tieleman. 2008. Distribution of amino acids in a lipid bilayer from computer simulations. *Biophys. J.* 94:3393–3404.

18. Hess, B., C. Kutzner, …, E. Lindahl. 2008. GROMACS 4: algorithms for highly efficient, load-balanced, and scalable molecular simulation. *J. Chem. Theory Comput.* 4:435–447.

19. Jorgensen, W. L., J. Chandrasekhar, …, M. L. Klein. 1983. Comparison of simple potential functions for simulating liquid water. *J. Chem. Phys.* 79:926–935.

20. Berger, O., O. Edholm, and F. Jähnig. 1997. Molecular dynamics simulations of a fluid bilayer of dipalmitoylphosphatidylcholine at full hydration, constant pressure, and constant temperature. *Biophys. J.* 72:2002–2013.

21. Kaminski, G. A., R. A. Friesner, …, W. L. Jorgensen. 2001. Evaluation and reparametrization of the OPLS-AA force field for proteins via comparison with accurate quantum chemical calculations on peptides. *J. Phys. Chem. B.* 105:6474–6487.

22. Kandt, C., W. L. Ash, and D. P. Tieleman. 2007. Setting up and running molecular dynamics simulations of membrane proteins. *Methods.* 41: 475–488.

23. Ferrenberg, A. M., and R. H. Swendsen. 1988. New Monte Carlo technique for studying phase transitions. *Phys. Rev. Lett.* 61:2635–2638.

24. Rokitskaya, T. I., N. I. Kolodkin, …, Y. N. Antonenko. 2011. Indolicidin action on membrane permeability: carrier mechanism versus pore formation. *Biochim. Biophys. Acta.* 1808:91–97.

25. Loken, C., D. Gruner, …, R. Van Zon. 2010. SciNet: lessons learned from building a power-efficient top-20 system and data centre. *J. Phys. Conf. Ser.* 256:012026.

Supporting Information

Chris Neale,[†,Δ] Jenny C.Y. Hsu, [Δ,‡] Christopher M. Yip, [Δ,‡] and Régis Pomès [†,Δ,*]

[†]Molecular Structure and Function, The Hospital for Sick Children, Toronto, ON, Canada; [Δ]Department of Biochemistry and [‡]Terrence Donnelly Centre for Cellular and Biomolecular Research, University of Toronto, Toronto, ON, Canada.
*Correspondence: pomes@sickkids.ca

Supplemental Methods

Simulation protocol. MD simulations were conducted using the methods and force field parameters outlined in our previous study of the insertion of a cationic arginine side chain analog near the center of a 1-palmitoyl-2-oleoyl-*sn*-glycero-3-phosphatidylcholine (POPC) lipid bilayer,[1] except as noted. Briefly, MD simulations were conducted with version 4.0.7 of the GROMACS simulation package.[2] The water model was TIP4P.[3] POPC was modeled by the Berger parameters.[4] Indolicidin was modeled by the OPLS-AA/L parameters.[5] The simulation system was neutralized with four chloride ions.

System setup and umbrella sampling. A neat POPC lipid bilayer with 64 lipids per leaflet and a total of 9162 water molecules was obtained from our previous work.[1] In a 50-ns equilibration of a neat bilayer system, the simulation box extended 10.8 (σ=0.1) nm along the bilayer normal (the Cartesian **z** dimension) and the area per lipid was 0.64 (σ=0.01) nm^2. A β-hairpin-like conformation of indolicidin was embedded in the bilayer using the inflategro routine,[6] according to our previously outlined protocol.[7] This peptide-insertion process was repeated 33 times, varying the axial position of the center of mass (COM) of the peptide relative to that of the lipid bilayer (the solute insertion depth, z, in 0.3 nm increments in the range -4.8$\leq z \leq$4.8 nm. This entire procedure was conducted for 30 initial peptide orientations according to the following definitions. The tilt of the long axis of the β-hairpin-like conformation, θ, was defined as the angle between the peptide vector $7P^{C\alpha} \rightarrow COM(4Y^{C\alpha}+11W^{C\alpha})$ and the positive Cartesian **z**-axis. Rotation about the long axis of the peptide, γ, was defined as the angle between the peptide vector $4Y^{C\alpha} \rightarrow 11W^{C\alpha}$ and the positive **x**-axis. The 30 initial peptide orientations were thus constructed for systematic combination of 0$\leq\theta\leq$180° in 45° increments and 0$\leq\gamma<$360° in 60° increments. This procedure generated starting conformations for a total of 990 restrained simulations.

Umbrella sampling (US) simulations at 300 K were conducted for 1.5 µs for each initial conformation and under the influence of each umbrella, except those simulations restrained to ±4.5 and ±4.8 nm, for which only 0.5 µs of simulation were conducted. During these simulations the peptide's immersion depth, z, was harmonically restrained to a specified value, z_i^0, in each

umbrella i, with a force constant, k_u, of 500 kJ/mol/nm^2. The orientation and conformation of the peptide were not restrained. Considering that each bilayer has two leaflets, these simulations yield a total of 60 distinct sets of US simulations for separate evaluations of the potential of mean force from bulk water to the center of the bilayer. These US simulations comprised 1.37 ms of simulation time. The peptide's immersion depth, z, was stored every 1 ps.

Extending a mixed selection of simulations to 10 µs/umbrella. We conducted sixty independent 1.5-µs simulations at each umbrella. Additionally, we extended two simulations at each umbrella to 10 µs each. We selected the two simulations at each umbrella that appeared best suited to their current immersion depth (and therefore most representative of equilibrium) based on a replica-exchange[8] formalism as follows (note that we did not simply extend two of the initial sets of US simulations, but rather mixed simulations at each umbrella from different initial sets).

For each conformation, $\mathbf{x}$, sampled in each simulation, we evaluated the total change in potential energy, Δ, that would occur if that conformation was switched with another conformation at a neighbouring value of z_i^0 according to Eq. S1:

$$\Delta = E_{\lambda_m}\left(\mathbf{x}^j\right) - E_{\lambda_m}\left(\mathbf{x}^i\right) - E_{\lambda_n}\left(\mathbf{x}^j\right) + E_{\lambda_n}\left(\mathbf{x}^i\right), \tag{S1}$$

where $E_{\lambda_m}\left(\mathbf{x}^j\right)$ is the potential energy of conformation $\mathbf{x}^j$ at $z_i^0 = \lambda_m$. We then evaluated the probability at which such an exchange would occur during replica exchange, P_{exchange}, according to Eq. S2:

$$P_{\text{exchange}} = \min\left[1, \exp\left(-\beta\Delta\right)\right], \tag{S2}$$

where $\beta = \left(k_B T\right)^{-1}$, k_B is the Boltzmann constant, and T is the absolute temperature. We evaluated Eq. S2 for each conformation from each simulation in the range $-4.2 \leq z_i^0 \leq 4.2$ nm against many conformations from each of the 30 simulations at each of the two neighbouring values of z_i^0. For this analysis, we used only the conformations from $1 < t < 1.5$ µs. Furthermore,

conformations were only compared when $|t_i\text{-}t_j|{\leq}20$ ns. When this evaluation required values from the simulations at $|z_i^0|{\geq}4.5$ nm, which only contained 0.5 µs of sampling, all values of $t{>}0.4$ µs were employed. We then selected, for further simulation, the simulation at each value of z_i^0 in the range $-4.2{\leq}z_i^0{\leq}4.2$ nm that had the lowest average sum value of P_{exchange}. This procedure was designed to pick a collection of simulations that would be least likely to migrate away from sampling at their current values of z_i^0 during replica exchange simulations and therefore be most representative of equilibrium. These 30 selected simulations covered the range $-4.2{\leq}z_i^0{\leq}4.2$ nm and were extended to 10 µs per umbrella, comprising a further 290 µs of simulation time.

Free energies and standard states. The values of z sampled in the US simulations were converted to free energy profiles, or potentials of mean force (PMFs) as outlined in our previous work.[7] To this end, recorded values of the solute insertion depth in the range $-4.8{\leq}z{\leq}4.8$ nm were distributed among 480 histogram bins and the WHAM calculation was performed with a tolerance of $1\text{x}10^{-5}$. This procedure was repeated for each set of US simulations. Each resulting PMF describes the free energy as a function of solute immersion depth, ΔG_z, from bulk water ($z{=}\text{-}4.8$ nm) across the bilayer center ($z{=}0$ nm) to bulk water ($z{=}4.8$ nm). Exploiting the symmetry of the system with respect to the plane at $z{=}0$ nm, we present the PMFs for the absolute value of z. Each PMF from water to the bilayer center was then shifted such that the average value of ΔG_z in the range $4.3{\leq}z{\leq}4.8$ nm equaled zero. Finally, the binding free energy, ΔG_{bind}, was determined by trapezoid integration of the PMF, as outlined previously,[7] in the range $0{<}z{\leq}4.3$ nm, thus placing the boundary of the bound state just beyond the point where the mean force becomes zero. The standard binding free energy, $\Delta G_{\text{bind}}^{\circ}$, was then computed by adjusting ΔG_{bind} such that the available volume is equal in the bound and unbound states, thus calculating $\Delta G_{\text{bind}}^{\circ}$ based on a volume-fraction partition coefficient, as outlined previously.[7]

PMFs of chloride along the bilayer normal were computed by constructing histograms of population density along the bilayer normal using the sampling from 1—1.5 µs per umbrella and then converting these probabilities, P_z, to free energies, ΔG_z, according to

$$\Delta G_z = -k_B T \times \ln(P_z) \,, \tag{S3}$$

where k_B is the Boltzmann constant and T is the absolute temperature. Standard binding free energies of chloride were computed using the same method that we used for indolicidin, except that PMFs were shifted to zero on the range $4.8 \leq z \leq 5.0$ nm and the bound state was defined as $0 < z \leq 4.8$ nm based on the PMFs presented in Fig. S7A.

Evaluating the change in the local volume enclosed within each bilayer leaflet. To classify structural perturbations of the lipid bilayer, we evaluated the volume enclosed within the bilayer defect in the leaflet in which the solute was embedded, V_ε. To this end, we conceptualized a cylinder of radium 0.1 nm, with its long axis along the global bilayer normal and its radial center at the center of mass of the solute. Additional cylinders, with radii increasing by 0.1 nm, were placed concentrically around the initial cylinder. Next, we computed the mean axial distance of lipid headgroup phosphorus atoms within each intervening hollow cylindrical segment (of width 0.1 nm) and subtracted the average axial displacement of phosphorus atoms from the bilayer center of mass obtained from simulations of a neat POPC bilayer, 1.934 nm (data not shown). Cylindrical segments that did not contain any phosphorus atoms were assigned the value of the next larger segment. The volume enclosed within the defect was then obtained separately for each leaflet by integrating the volumes of the perturbations in each cylindrical segment out to a radial distance of 1.5 nm from the center of mass of the solute. Values of V_ε are shown such that negative values represent local invaginations of the bilayer toward its center.

This method will provide artificially large negative values of V_ε if lipids, which are assigned to their initial leaflet, are mislocated due to lipid flip-flop. We therefore assessed lipid flip-flop by searching for conformations in which the phosphorus atom of any lipid crossed the bilayer center by more than 0.9 nm. Because bona-fide lipid flip-flop occurred in only one trajectory (at $z_i^0 = 0.9$ nm, data not shown), we simply omitted that trajectory from our computation of V_ε.

Counting peptide-lipid ion pairs. We computed the number of peptide-lipid salt bridges, N_{SB}. An interaction was counted whenever at least one lipid phosphocholine heavy atom was within

0.435 nm of a designated protein charge. Protein charges were represented by (i) the (N-terminal) nitrogen atom of Ile1, (ii) the N_ζ atom of Lys5, or the C_ζ atom of (iii) Arg12 or (iv) Arg13. The following three examples are provided for clarity: if the N_ζ atom of Lys5 was within the cutoff of two heavy atoms of one lipid phosphocholine group, only one interaction was counted; if the N_ζ atom of Lys5 was within the cutoff of two phosphocholine heavy atoms, both from different lipid molecules, two interactions were counted; if the heavy atoms of one lipid phosphocholine group were within the cutoff of both the N_ζ atom of Lys5 and the C_ζ atom of Arg12, two interactions were counted. The counts were larger but qualitatively similar using a cutoff of 0.6 nm (data not shown).

Counting water molecules in the bilayer core. We computed the number of water molecules within the hydrophobic core of the bilayer, N_{water}. A water molecule was counted whenever its oxygen atom was within 0.5 nm of the center of the bilayer. The counts were larger but qualitatively similar using a cutoff of 1.0 nm (data not shown).

Peptide end-to-end distance. We computed the end-to-end distance of the peptide, EED, as the distance between the C_α atoms of Ile1 and Arg13.

Supplemental Results

Utility of massively repeated simulations. Our initial sampling comprised 60 independent sets of US simulations from bulk water to the bilayer center, each initiated with a different conformation (see Supplemental Methods). In the main article, we showed that the standard binding free energy, ΔG_{bind}°, evaluated based on a 50-ns sampling window, undergoes a systematic drift with increasing equilibration time, t_{eq}. Because simulation studies most often employ a single or relatively few repeat simulations at each umbrella, we emphasize the disparity of the convergence profiles among independent US simulations in Fig. S1A. Furthermore, Fig. S1B traces the PMFs computed from the last 0.5 μs of sampling, again shown separately for each US simulation. The variance of the ΔG_{bind}° estimates is depicted numerically in Table S1. Importantly, four of the sixty sets of US simulations (7%) yield an estimate of ΔG_{bind}° that deviates from the mean value by > 10 kcal/mol (Table S1). From this data, we conclude that the convergence profile from a single US simulation may not always be a good estimate of *bona fide* convergence.
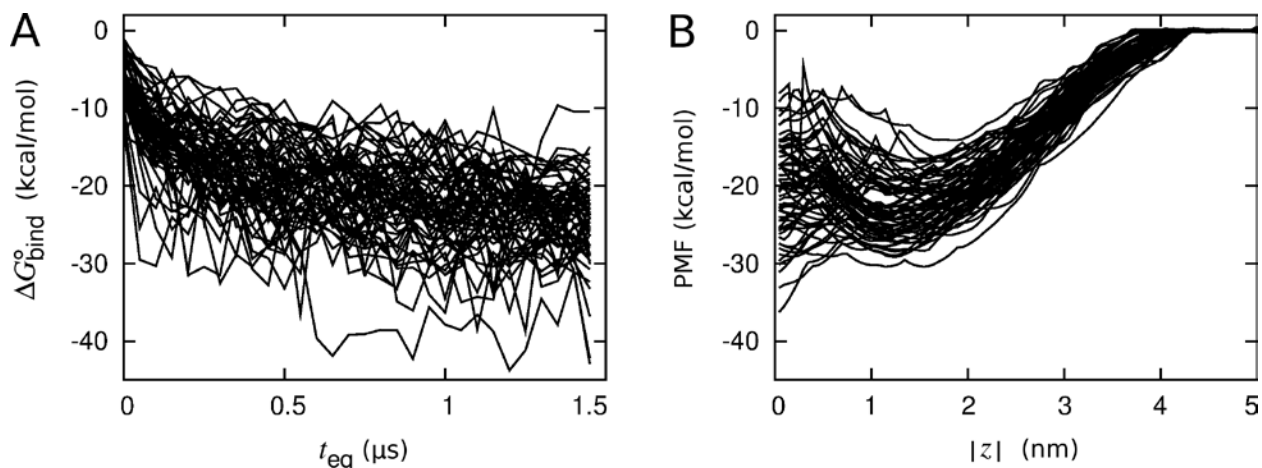

Figure S1. Convergence of the PMF for indolicidin partitioning into a POPC bilayer. The data is the same as in Fig. 1 in the main manuscript, except that this Figure depicts the profiles obtained from each individual US simulation.

Table S1: Standard binding free energies, $\Delta G_{\text{bind}}^{\circ}$, of indolicidin to a POPC lipid bilayer.

Sample (μs)	$\Delta G_{\text{bind}}^{\circ}$ (kcal/mol)	
	$\mu \pm \sigma_M$	Values from component sets of US simulations
1.45→1.50	-24 ± 5	-10, -15, -16, -17, -17, -17, -18, -19, -19, -20, -20, -20, -20, -20, -20, -21, -21, -21, -21, -22, -22, -22, -22, -23, -23, -23, -23, -24, -24, -24, -24, -24, -24, -24, -24, -24, -25, -25, -25, -25, -26, -26, -26, -26, -28, -28, -28, -28, -29, -29, -30, -30, -30, -31, -32, -33, -37, -42, -43

Comparison of convergence in the initial US simulations with 1.5 μs/umbrella and the extended US simulations with 10 μs/umbrella. It is important to note that our 10-μs/umbrella simulations are not mere continuations of two of the initial 1.5-μs/umbrella simulations. Rather, we used all of the data from the initial 1.37 ms of sampling to identify simulations at each umbrella that appeared best suited to their current immersion depth (see Supplemental Methods). Therefore, our finding that these US simulations attained convergence after 4 μs/umbrella is inextricably linked to the conduction of massively repeated simulations followed by a selection algorithm based on replica exchange. It does not necessarily follow that each initial set of US simulations is likely to attain convergence after 4 μs/umbrella.

Water penetration. In the main letter, we noted that indolcidin draws water molecules into the hydrophobic core of the bilayer. Surprisingly, the number of water molecules within 0.5 nm of the bilayer core converged rapidly (Fig. S2).
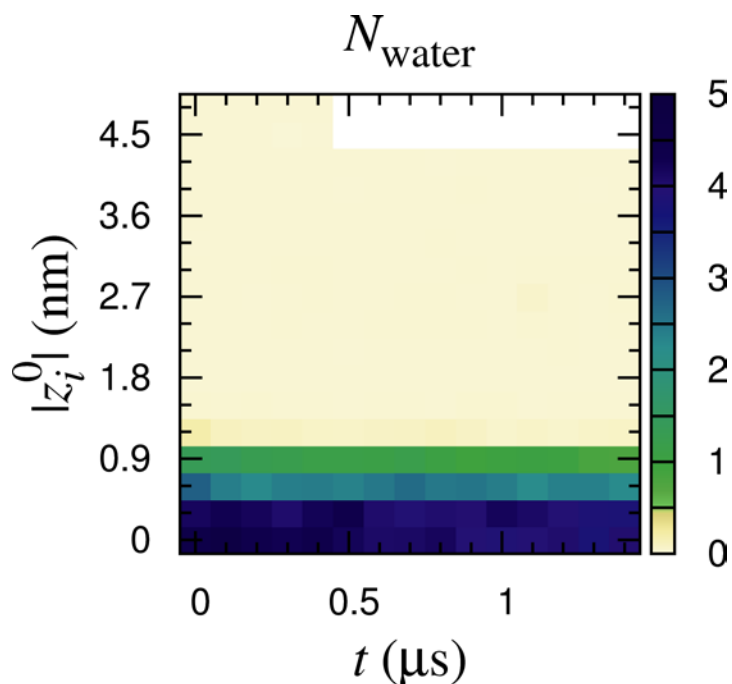
Figure S2. Average number of water molecules in the bilayer core, N_{water}, as a function of simulation time, t, and umbrella center, $\left|z_i^0\right|$. There is no sampling for $t>0.5$ μs at $\left|z_i^0\right|\geq4.5$ nm.

The largest water pore that formed in our simulations brought 36 water molecules within 0.5 nm of the bilayer center at $\left|z_i^0\right|=0.6$ nm (Fig. S3). Even when there were relatively few water molecules in the bilayer core, they sometimes adopted configurations approaching a pore (Fig. S4). Finally, the distortion of the bilayer structure that occurs upon deep indolicidin insertion is highlighted in Fig. S5.
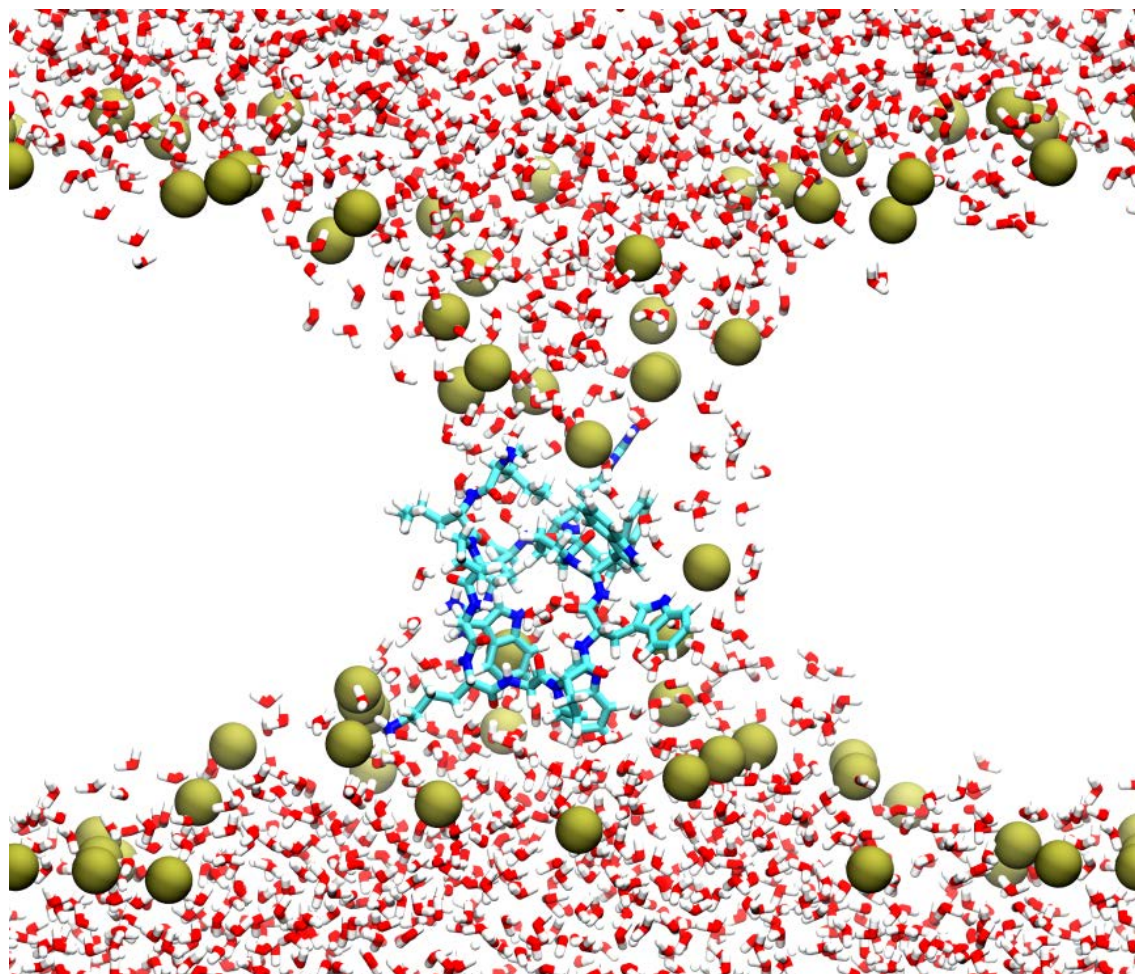
Figure S3. Largest water pore formed in our simulations. Lipid headgroup phosphorus atoms are shown in brown.
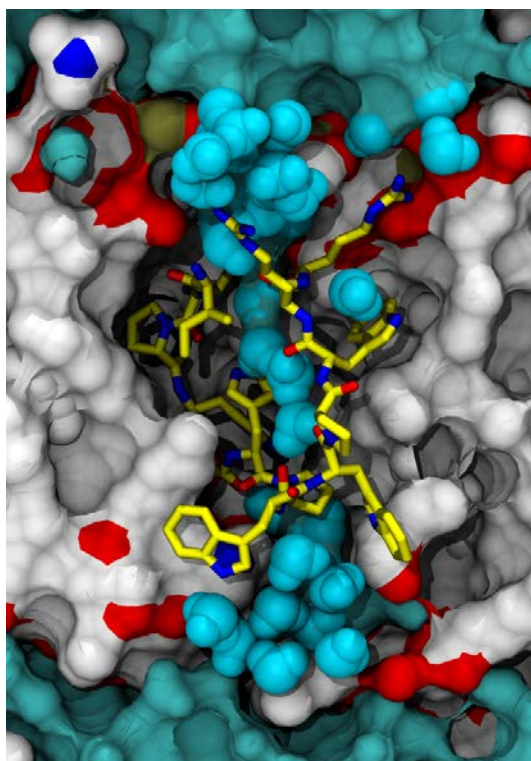
Figure S4. Relatively few water molecules are required to traverse the bilayer in the presence of indolicidin. Water is shown in cyan.
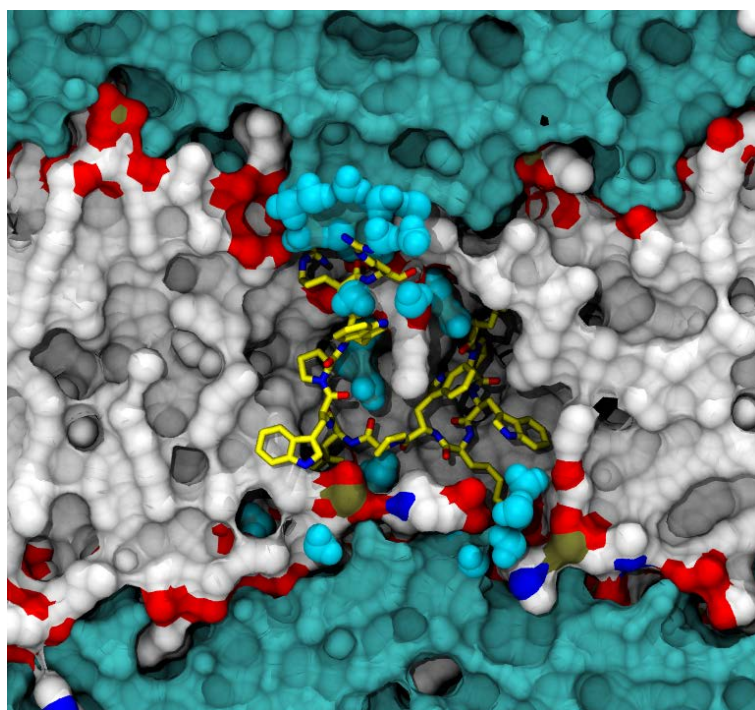

Figure S5. Bilayer distortion upon indolicidin insertion.

Chloride penetration. It has been suggested that indolicidin does not form pores in uncharged lipid vesicles, but rather acts as an organic anion carrier.[9] Therefore, we evaluated the bilayer insertion of chloride in our simulations. These ions approached within 1.0 nm of the bilayer center in 14 simulations, all of which were conducted at $\left|z_i^0\right| \leq 0.9$ nm. An example of such a binding event is depicted in Fig. S6. However, no chloride ions were ever found within 0.5 nm of the bilayer center, suggesting that there were no crossing events.
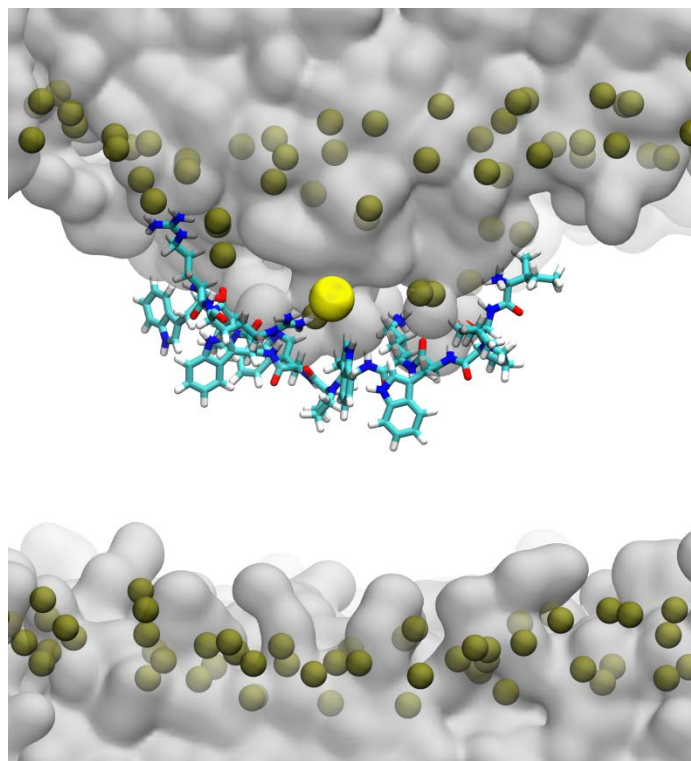
Figure S6: Chloride binds membrane-bound indolicidin. Chloride (yellow), lipid headgroup phosphorus atoms (brown), water (grey surface), and indolicidin (sticks) are highlighted.

To directly assess the bilayer permeation of chloride in the presence of indolicidin, we computed the PMFs of chloride along the bilayer normal for each value of $\left|z_i^0\right|$ (Fig. S7A). From these PMFs we computed the standard binding free energy, $\Delta G_{\text{bind}}^\circ$, of chloride to the lipid bilayer/peptide as a function of $\left|z_i^0\right|$ (Fig. S7B).
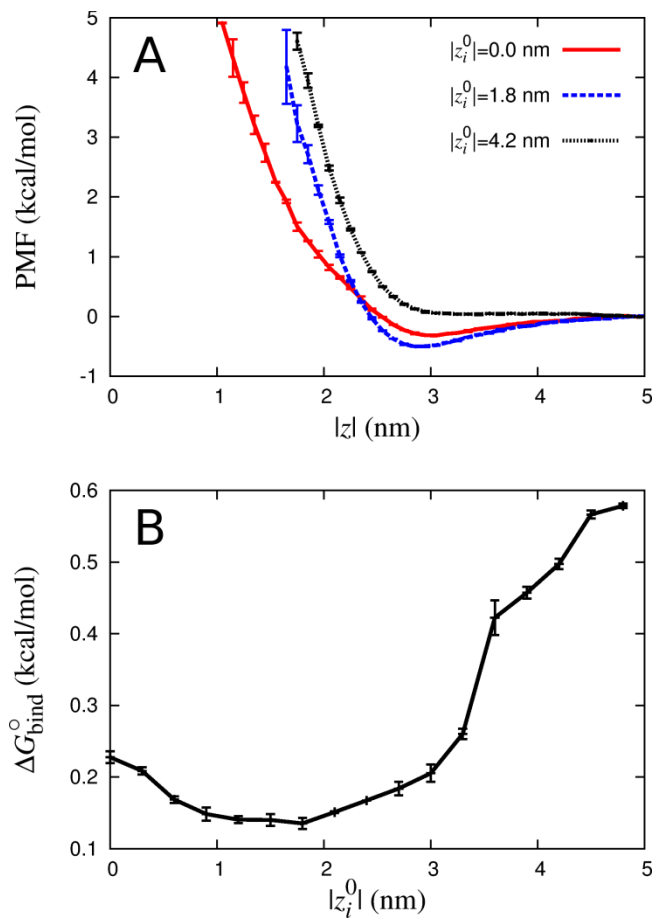
Figure S7: Free energy of chloride along the bilayer normal as a function of peptide $\left|z_i^0\right|$. (A) Representative PMFs of chloride along the bilayer normal for three different values of peptide $\left|z_i^0\right|$. (B) $\Delta G_{\mathrm{bind}}^{\circ}$ of chloride as a function of peptide $\left|z_i^0\right|$. Standard deviations were computed by dividing the US simulations into two groups.

Our results indicate that indolicidin is not capable of acting as a chloride carrier (Fig. S7A), although membrane-bound indolicidin does increase the membrane binding of chloride (Fig. S7B). We note that our simulations are unable to address whether monomeric indolicidin is an organic anion carrier or whether multimeric indolicidin is capable of carrying chloride across a lipid bilayer.

Comparison to the PMFs of Yeh *et al.* As noted in the main letter, the potentials of mean force (PMFs) that we computed in this work are strikingly different from those computed by Yeh *et al.*, who used different force field parameters, substantially shorter simulations, and a different

method to generate initial conformations.[10] In particular, we embedded the peptide into the hydrated bilayer system separately for each umbrella (using the inflategro routine,[6] see Supplemental Methods) such that the displacement between the COMs of the peptide and the bilayer, z, coincided with the umbrella center, z_i^0, at time t=0. In contrast, Yeh *et al.* started each of their constituent umbrella sampling (US) simulations with the peptide in bulk water, approximately 5 nm away from the COM of the bilayer along its normal.[10] In this way, the initial conditions of our simulations and those of Yeh *et al.* likely biased the short-time sampling of the peptide toward bilayer insertion and aqueous solvation, respectively.

To evaluate the influence of initial conformation on the PMF at relatively short simulation times, we repeated our US simulations 30 times using initial conformations in which indolicidin was placed in bulk water with a COM displacement from the bilayer of 4.2 nm. US was then conducted for 25 ns per umbrella. The PMF obtained after discarding the first 10 ns as equilibration is shown in Fig. S8, where it is labeled as "approach (10—25 ns)". This PMF is qualitatively similar to the one presented by Yeh *et al.*[10] in that both PMFs indicate that indolicidin does not insert into the lipid bilayer although, in comparison, the PMF that we computed indicates that bilayer adsorption is more favourable by about 3 kcal/mol (Fig. S8, Table S2, and Yeh *et al.*[10]). Importantly, the PMF that we computed from similarly short simulations using the same force field but a different method of peptide insertion differs substantially, indicating that indolicidin partitions into the lipid bilayer (Fig. S8). Finally, when we increase the simulation time, this insertion becomes more favourable (Fig. S8 and Table S2).

Together, the three PMFs in Fig. S8 suggest that simulations of Yeh *et al.*[10] may not have attained convergence, complicating the comparison of PMFs in these two studies because sampling convergence is necessary for force field evaluation.
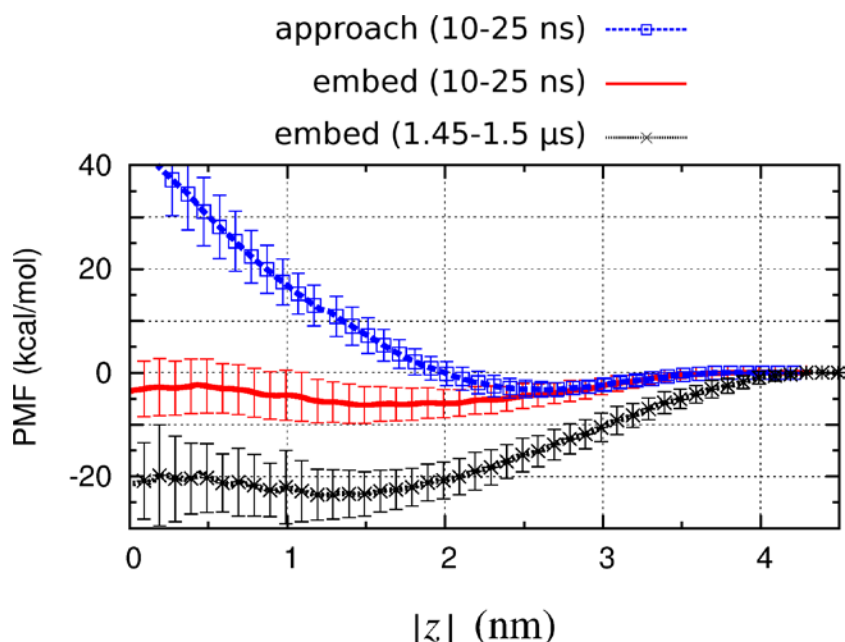
Figure S8: Comparison of PMFs obtained with different methods of generating the starting conformations and different amounts of equilibration. PMFs were generated from 10 ns of equilibration and 15 ns of sampling per umbrella based on (i) initial conformations in which the peptide was placed in bulk water (the "approach" method of Yeh *et al.*;[10] broken blue line with squares), or (ii) initial conformations in which the peptide was embedded in the lipid bilayer separately according to each value of z_i^0 (the "embed" method utilized in this work; solid red line). For comparison, also shown is (iii) the PMF generated from 1.45 μs of equilibration and 50 ns of sampling based on the "embed" method (dotted black line with x symbols). Error bars represent the standard deviation of 30 and 60 repeat simulations for shorter and longer simulations, respectively, each of which was used to construct a separate PMF.

Table S2: Free energy values computed from the individual PMFs used to construct Fig. S8.

Dataset	ΔG_{bind}° (kcal/mol)	min(PMF) (kcal/mol)[a]	z of min(PMF) (nm)[b]
Approach (10—25 ns)	-2.4 ± 1.5	-3.8 ± 1.6	2.7 ± 0.2
Embed (10—25 ns)	-6.6 ± 3.4	-8.0 ± 3.5	1.4 ± 0.9
Embed (1.45—1.5 μs)	-24.4 ± 4.8	-26.0 ± 4.9	1.0 ± 0.6

[a]The minimum value of the PMF after adjusting the PMF to zero in bulk water.
[b]The location of the minimum value of the PMF.

Supplemental Acknowledgements

Supplemental References

1.	Neale, C.; Madill, C.; Rauscher, S.; Pomès, R., Accelerating convergence in molecular dynamics simulations of solutes in lipid membranes by conducting a random walk along the bilayer normal. *J. Chem. Theory Comput.* **2013,** *9* (8), 3686-3703.
2.	Hess, B.; Kutzner, C.; van der Spoel, D.; Lindahl, E., GROMACS 4: algorithms for highly efficient, load-balanced, and scalable molecular simulation. *J. Chem. Theory Comput.* **2008,** *4* (3), 435-447.
3.	Jorgensen, W. L.; Chandrasekhar, J.; Madura, J. D.; Impey, R. W.; Klein, M. L., Comparison of simple potential functions for simulating liquid water. *J. Chem. Phys.* **1983,** *79* (2), 926-935.
4.	Berger, O.; Edholm, O.; Jähnig, F., Molecular dynamics simulations of a fluid bilayer of dipalmitoylphosphatidylcholine at full hydration, constant pressure, and constant temperature. *Biophys. J.* **1997,** *72* (5), 2002-2013.
5.	Kaminski, G. A.; Friesner, R. A.; Tirado-Rives, J.; Jorgensen, W. L., Evaluation and reparametrization of the OPLS-AA force field for proteins via comparison with accurate quantum chemical calculations on peptides. *J. Phys. Chem. B* **2001,** *105* (28), 6474-6487.
6.	Kandt, C.; Ash, W. L.; Tieleman, D. P., Setting up and running molecular dynamics simulations of membrane proteins. *Methods* **2007,** *41* (4), 475-488.
7.	Neale, C.; Bennett, W. F. D.; Tieleman, D. P.; Pomès, R., Statistical convergence of equilibrium properties in simulations of molecular solutes embedded in lipid bilayers. *J. Chem. Theory Comput.* **2011,** *7* (12), 4175-4188.
8.	Ferrenberg, A. M.; Swendsen, R. H., New Monte Carlo technique for studying phase transitions. *Phys. Rev. Lett.* **1988,** *61* (23), 2635-2638.
9.	Rokitskaya, T. I.; Kolodkin, N. I.; Kotova, E. A.; Antonenko, Y. N., Indolicidin action on membrane permeability: Carrier mechanism versus pore formation. *BBA-Biomembranes* **2011,** *1808* (1), 91-97.
10.	Yeh, I.-C.; Ripoll, D. R.; Wallqvist, A., Free energy difference in indolicidin attraction to eukaryotic and prokaryotic model cell membranes. *J. Phys. Chem. B* **2012,** *116* (10), 3387-3396.